Magnetic Resonance in Medicine 50:263–274 (2003)

Functional Magnetic Resonance Imaging Based on Changes in Vascular Space Occupancy

Hanzhang Lu,[1–3]* Xavier Golay,[1,3] James J. Pekar,[1,3] and Peter C.M. van Zijl[1,3]*

During brain activation, local control of oxygen delivery is facilitated through microvascular dilatation and constriction. A new functional MRI (fMRI) methodology is reported that is sensitive to these microvascular adjustments. This contrast is accomplished by eliminating the blood signal in a manner that is independent of blood oxygenation and flow. As a consequence, changes in cerebral blood volume (CBV) can be assessed through changes in the remaining extravascular water signal (i.e., that of parenchymal tissue) without need for exogenous contrast agents or any other invasive procedures. The feasibility of this vascular space occupancy (VASO)-dependent functional MRI (fMRI) approach is demonstrated for visual stimulation, breath-hold (hypercapnia), and hyperventilation (hypocapnia). During visual stimulation and breath-hold, the VASO signal shows an inverse correlation with the stimulus paradigm, consistent with local vasodilatation. This effect is reversed during hyperventilation. Comparison of the hemodynamic responses of VASO-fMRI, cerebral blood flow (CBF)-based fMRI, and blood oxygenation level-dependent (BOLD) fMRI indicates both arteriolar and venular temporal characteristics in VASO. The effect of changes in water exchange rate and partial volume contamination with CSF were calculated to be negligible. At the commonly-used fMRI resolution of 3.75 × 3.75 × 5 mm^3, the contrast-to-noise-ratio (CNR) of VASO-fMRI was comparable to that of CBF-based fMRI, but a factor of 3 lower than for BOLD-fMRI. Arguments supporting a better gray matter localization for the VASO-fMRI approach compared to BOLD are provided. Magn Reson Med 50:263–274, 2003. © 2003 Wiley-Liss, Inc.

Key words: cerebral blood volume; fMRI; visual stimulation; microvascular; water relocation; exchange; hyperventilation; breath-hold; hemodynamic response; BOLD; cerebral blood flow; VASO

During the last decade, functional MRI (fMRI) has revolutionized the field of cognitive neuroscience. This is a consequence of its capability to provide noninvasive spatial mapping of the hemodynamic response to neuronal activity (1–3). To date, virtually all fMRI studies in human subjects have been based on the measurement of local changes in the oxygenation state of hemoglobin, which affects the MRI signal by changing the local magnetic field in the image volume elements (voxels). This so-called blood oxygenation level-dependent (BOLD) phenomenon (1,4) reflects the combined effect of many physiological parameters, including oxygen extraction ratio, cerebral metabolic rate of oxygen, cerebral blood flow (CBF) and volume (CBV), hematocrit, and initial arterial oxygenation fraction (4–6). One drawback of the BOLD approach is that the altered oxygenation state of hemoglobin not only influences MRI signals in and around the microvessels close to the sites of neuronal activation, but also in and around the large veins draining from these areas (7–10). This problem is especially apparent at low magnetic field strengths (1.5 Tesla), at which most fMRI studies are conducted, and persists at intermediate (3–4 Tesla) and higher fields (9). Although the availability of improved spatial resolution at higher magnetic field strengths allows the actual areas of activation to be better localized, it would be extremely useful to have a method in which the contrast would arise predominantly from the microvessels that are expanding due to local neuronal activation.

The brain vasculature is under dual mechanistic control (11). The diameters of larger vessels of the cerebral inflow tract are under sympathetic regulation, and are considered to be unimportant for local regulation of flow during activation. On the other hand, the diameters of small intraparenchymal vessels (100–200 μm) are influenced by the demand for homeostasis of the microevironment. Such local neurovascular coupling is mediated by vasoactive compounds, such as CO_2, NO, prostaglandin, and K^+ (11–13). An fMRI approach that reflects activation-related microvascular regulation is expected to show effects in local parenchyma (tissue + microvasculature), but not in large vessels. To achieve contrast that is dependent on vascular space occupancy (VASO), we designed a technique in which the blood signal is selectively nulled. This was accomplished by taking advantage of the fact that MRI radiofrequency (RF) pulses can invert the longitudinal equilibrium magnetization of water from parallel with respect to the magnetic field to antiparallel, after which the inverted magnetization returns exponentially to equilibrium with the longitudinal relaxation time constant T_1 (Fig. 1). Because T_1 differs between blood and tissue, the times at which their magnetizations cross zero differ, and, when images are acquired at the time of blood nulling, sufficient gray matter tissue magnetization remains for MRI detection (Fig. 1).

Here we demonstrate the feasibility of this VASO-fMRI approach during vasodilatation (visual stimulation and breath-hold) and vasoconstriction (hyperventilation) manipulations in humans at 1.5 T. In addition, an event-related visual stimulation experiment was performed to compare the hemodynamic and contrast-to-noise-ratio (CNR) characteristics of VASO with that of conventional BOLD-fMRI and a CBF-based fMRI approach using pulsed

[1]Department of Radiology, Johns Hopkins University School of Medicine, Baltimore, Maryland.

[2]Department of Biomedical Engineering, Johns Hopkins University School of Medicine, Baltimore, Maryland.

[3]F.M. Kirby Research Center for Functional Brain Imaging, Kennedy Krieger Institute, Baltimore, Maryland.

Grant sponsor: NIH; Grant number: NS37664 (NINDS); Grant sponsor: National Center for Research Resources; Grant number: RR15241.

*Correspondence to: Peter C.M. van Zijl or Hanzhang Lu, Dept. of Radiology, Johns Hopkins University School of Medicine, 217 Traylor Bldg., 720 Rutland Ave., Baltimore, MD 21205. E-mail: pvanzijl@mri.jhu.edu

Received 5 December 2002; revised 10 March 2003; accepted 30 March 2003.

DOI 10.1002/mrm.10519
Published online in Wiley InterScience (www.interscience.wiley.com).

arterial spin labeling (PASL-fMRI). Finally, fMRI data were acquired at high resolution to compare the spatial specificities of the VASO and BOLD methods.

METHODS

Description of the Method

Figure 1 shows the basic MRI pulse sequence for VASO-fMRI. After nonselective inversion of the starting longitudinal magnetization, $M(0)$, from parallel to the magnetic field to antiparallel, the parenchymal components relax back to equilibrium. Because T_1 differs between blood and tissue, the point at which the magnetization crosses through zero differs. Longitudinal magnetization cannot be detected, but when, at a time t = TI, such an inversion experiment is followed by excitation of transverse magnetization (which is detectable), the effects of the inversion preparation determine the starting signal magnitude (Fig. 1). This signal decays exponentially with the transverse relaxation time, which is described by T_2^* for gradient-echo imaging and T_2 for spin-echo imaging. When a gradient-echo pulse sequence is used for image acquisition with echo time TE, the signal dependence is:

$$S \sim M(\mathrm{TI}) \cdot e^{-\mathrm{TE}/T_2^*} = M(0) \cdot [1 - 2e^{-\mathrm{TI}/T_1} + e^{-\mathrm{TR}/T_1}] \cdot e^{-\mathrm{TE}/T_2^*} \quad [1]$$

in which TR is the time needed for a single MRI acquisition (Fig. 1). Thus, for VASO-fMRI to be successful, $M_{blood,i}(\mathrm{TI})$ must be zero, while $M_{tissue}(\mathrm{TI})$ should preferably be as large as possible. The method must be optimized to ensure that the blood signal nulling is achieved in a manner that is insensitive to changes in blood flow velocity (to avoid inflow artifacts) and blood oxygenation during brain activation. The technique was made insensitive to blood flow velocity changes by inverting magnetization in a spatially nonselective manner. Independence of blood oxygenation for T_1 has been reported (14). Since T_1 depends on the magnetic field, blood T_1 for each particular field strength must be determined to optimize TI for nulling. In addition, to minimize residual BOLD effects, the time of detection of the maximum MRI signal after excitation (the TE) was kept as short as possible.

Theory of VASO Signal Changes

The vascular-space-occupancy of a particular microvessel, ξ_i is defined as:

$$\xi_i = \mathrm{CBV}_i / V_{par} = \mathrm{CBV}_i \Big/ \left(V_{tissue} + \sum_i \mathrm{CBV}_i \right)$$

$$i = \text{arteriole, capillary or venule} \quad [2]$$

in which V_{par} indicates parenchymal volume (ml tissue/g tissue) and CBV is the cerebral blood volume (ml blood/g tissue). Thus, the units of ξ are ml blood/ml parenchyma. Notice that CBV is the parenchymal blood volume and not the cerebrovascular volume (CVV), in which the large vessels and parenchyma are included (15). For pure brain parenchyma (perfused tissue), the MRI signal (S) is proportional to the sum of the magnetization (M) contributions of the microvessels (i = arterioles, capillaries, and venules) and pure tissue. For a spatially nonselective inversion recovery experiment followed, at time TI, by slice-selective excitation and gradient-echo detection, we have

$$S_{par} = S_{blood} + S_{tissue} \sim \left(\sum_i \xi_i C_{blood} \right) \cdot M_{blood,i}(\mathrm{TI}) \cdot e^{-\mathrm{TE}/T^*_{2,blood,i}} + \left(C_{par} - \sum_i \xi_i C_{blood} \right) \cdot M_{tissue}(\mathrm{TI}) \cdot e^{-\mathrm{TE}/T^*_{2,tissue}} \quad [3]$$

in which C is the water density of microvascular blood (or tissue) in ml water/ml blood (or tissue), as defined in our previous paper (16), $T^*_{2,\mathrm{blood,i}}$ and $T^*_{2,\mathrm{tissue}}$ are the effective transverse relaxation times of blood and tissue, respectively. For flow-independent inversion and proper blood nulling independent of oxygenation (i.e., $M_{blood,i}(\mathrm{TI}) = 0$), Eq. [3] can be rewritten as:

$$S_{par} \sim \left(C_{par} - \sum_i \xi_i C_{blood} \right) \cdot M_{tissue}(\mathrm{TI}) \cdot e^{-\mathrm{TE}/T^*_{2,tissue}}. \quad [4]$$

Defining $\xi = \Sigma_i \xi_i$ as the total microvascular space occupancy, the fractional parenchymal signal change during neuronal activity can then be derived to be:

$$\frac{\Delta S}{S} = \frac{S^{act}_{par} - S^{rest}_{par}}{S^{rest}_{par}} = \frac{(C_{par} - \xi^{act} C_{blood}) e^{-\mathrm{TE}/T^{*,act}_{2,tissue}} - (C_{par} - \xi^{rest} C_{blood}) e^{-\mathrm{TE}/T^{*,rest}_{2,tissue}}}{(C_{par} - \xi^{rest} C_{blood}) e^{-\mathrm{TE}/T^{*,rest}_{2,tissue}}}. \quad [5]$$

Thus, the VASO signal change includes the effect of extravascular BOLD changes (signal increase upon activation). Rewriting $e^{-\mathrm{TE}/T^{*act}_{2,tissue}} = e^{-\mathrm{TE}/T^{*rest}_{2,tissue}} \cdot e^{-\Delta(1/T^*_{2,tissue})\mathrm{TE}}$ and assuming that, at the short TE and low field strength used, the effect of the extravascular BOLD T_2^* change in tissue can be neglected, the fractional signal change then simplifies to:

$$\frac{\Delta S}{S} = \frac{(\xi^{rest} - \xi^{act}) C_{blood}}{(C_{par} - \xi^{rest} C_{blood})} = \frac{-\Delta\xi \cdot C_{blood}}{(C_{par} - \xi^{rest} C_{blood})}. \quad [6]$$

Neuronal activity causes microvascular vasodilatation, resulting in increased VASO, i.e., $\xi^{act} > \xi^{rest}$. Therefore, in contrast to the BOLD effect, a negative signal change is expected in VASO fMRI (Fig. 2d).

Calibration for Blood Signal Nulling

The main requirement to be fulfilled for successful VASO-fMRI is that signal nulling can be achieved independently of differences in oxygenation between arteries, capillaries, and veins. To determine an accurate TI for blood nulling, we measured blood T_1 values at 1.5 Tesla for arterial and venous blood under physiological conditions in a perfusion phantom (17,18). Blood temperature was maintained at 37°C and was kept circulating at 3.1 ml/min to prevent coagulation. The oxygenation saturation fraction (Y) of blood was manipulated by gas mixture (N_2 and O_2) and

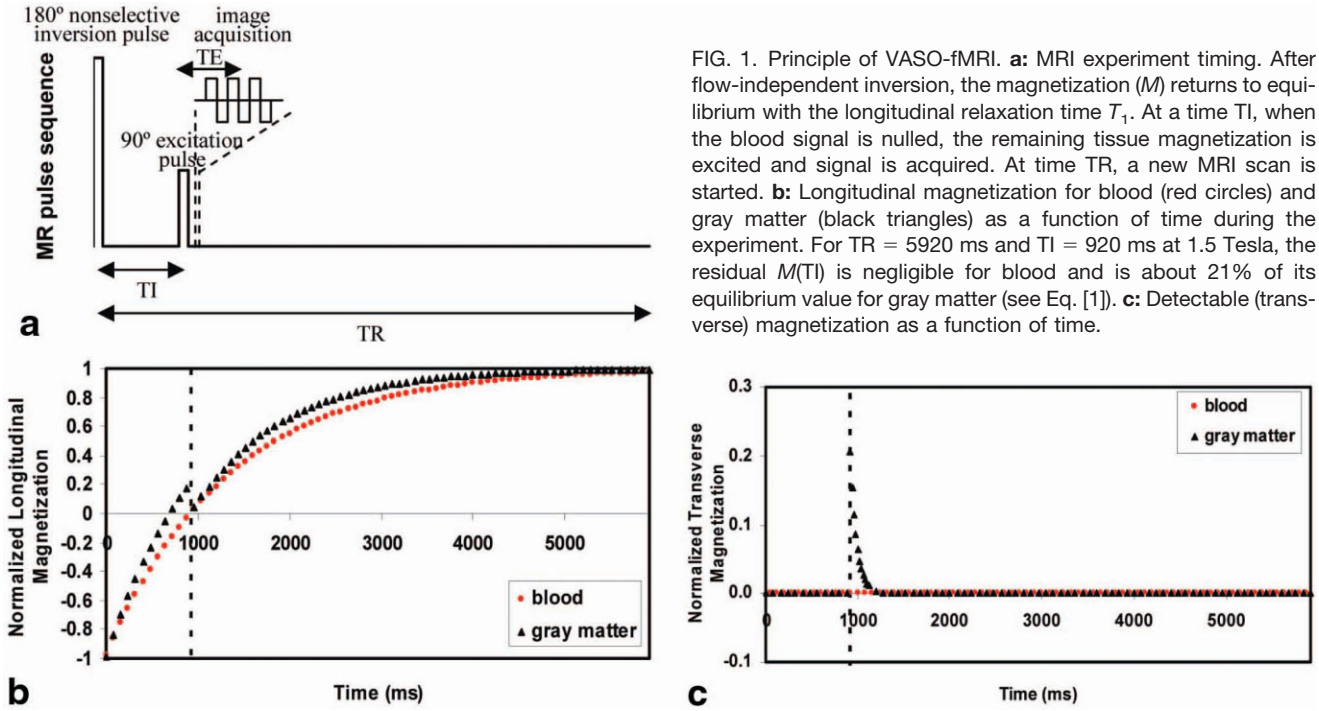

FIG. 1. Principle of VASO-fMRI. **a:** MRI experiment timing. After flow-independent inversion, the magnetization (M) returns to equilibrium with the longitudinal relaxation time T_1. At a time TI, when the blood signal is nulled, the remaining tissue magnetization is excited and signal is acquired. At time TR, a new MRI scan is started. **b:** Longitudinal magnetization for blood (red circles) and gray matter (black triangles) as a function of time during the experiment. For TR = 5920 ms and TI = 920 ms at 1.5 Tesla, the residual M(TI) is negligible for blood and is about 21% of its equilibrium value for gray matter (see Eq. [1]). **c:** Detectable (transverse) magnetization as a function of time.

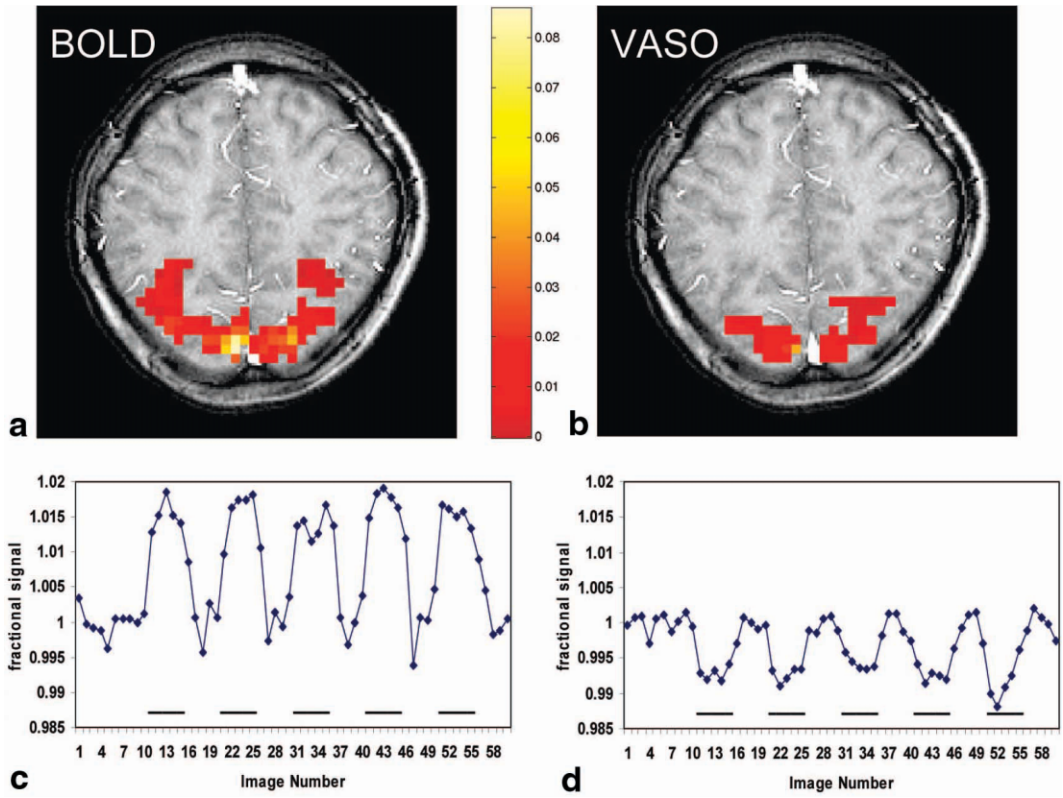

FIG. 2. Visual activation maps ($P < 0.005$) for BOLD-fMRI (**a**) and VASO-fMRI (**b**). Color bar indicates amplitude of fractional signal changes (positive for BOLD and negative for VASO). Activation data are overlaid on a high-resolution anatomical image. Spatially similar activation patterns are detected by both fMRI methods, although BOLD has more activated voxels than VASO. **c** and **d:** Average time-courses (N = 5) of the activated voxels for BOLD- and VASO-fMRI, respectively. Solid bars below the plots denote the timing of the stimulus paradigm. At this low spatial resolution ($4 \times 4 \times 10$ mm^3), a 1.5% signal increase and a 0.7% signal decrease are seen for BOLD and VASO, respectively.

monitored with a blood analyzer (Radiometer America Inc., Westlake, OH). For convenience, we used bovine blood, which is known to have hemoglobin content, erythrocyte size, and diffusional permeability comparable to human blood (19). For T_1 measurements, an inversion recovery spin-echo imaging sequence was used with the following parameters: field of view (FOV) = 20 × 20 mm^2, TE = 9 ms, slice thickness = 10 mm, matrix = 64 × 64. Nine inversion times (TIs) were used (10, 50, 100, 250, 500, 1000, 2000, 3000, 5000 ms) with TR adjusted accordingly to maintain the same recovery time after excitation (5 s). When assuming perfect inversion efficiency (body coil, adiabatic inversion), the magnetization at the end of TI is described by M(TI) in Eq. [1]. For each voxel, a three-parameter fit of the signal intensities as a function of TI was performed. The measured T_1 values were 1355 ± 38 ms (SD) and 1390 ± 44 ms for fully oxygenated and deoxygenated blood (47% oxygenated), respectively, the magnitudes of which are indistinguishable within experimental error. To confirm this range for humans, we also determined T_1 in the sagittal sinus, giving 1389 ± 35 ms, in close agreement with the deoxygenated phantom blood results. Since arteriolar and precapillary vessels are expected to be the main contributors to vascular expansion (11), we used T_1 = 1350 ms to calculate the TI values for blood nulling under our experimental MRI conditions. For a typical parenchymal gray matter voxel with about 95% tissue and 5% blood, the residual arterial, capillary, and venous contributions can then be calculated to be 0.008%, 0.072%, and 0.183%, respectively, of the total signal.

Functional Studies

All subjects (N = 17 (eight females and nine males)) gave informed consent before participating in the study. The experiments were performed on a 1.5 T whole-body scanner (Philips Medical System, Best, The Netherlands). A body coil was used for RF transmission in all scans. Single-shot, gradient-echo echo-planar imaging (GE-EPI) with a flip angle (FA) of 90° was used for data acquisition. A high-resolution (FOV = 240 × 240 mm^2, matrix = 256 × 256) scan was also obtained for anatomical reference. For VASO-fMRI, flow-velocity-insensitive blood nulling was achieved by using the body coil for non-slice-selective inversion, followed by TI values of 920 ms and 665 ms for experiments with repetition times (TRs) of 5920 ms and 2000 ms, respectively. TE was shortened as much as possible to minimize BOLD contamination. When a 60–65% half scan was used (20), TE values of 10–11 ms, respectively, could be achieved. For BOLD fMRI, the TE was 50 ms to maximize the signal contrast. The pulsed arterial spin labeling (PASL) method used for CBF-fMRI was the transfer insensitive labeling technique (TILT) approach (21). The principles used in this sequence are similar to those of the EPI-STAR (signal targeting with alternating radio frequency) technique (22), but there is less contamination from magnetization transfer effects. An inversion delay of 1200 ms was used to reduce contributions from vascular water. The labeling slab thickness was 10 cm, and the gap between the labeling slab and imaging slice was 5 mm. TE was 11 ms.

fMRI experiments were performed during the following physiological manipulations:

Visual Stimulation

A blue-yellow flashing checkerboard (frequency = 8 Hz, visual angle = 25°), was projected onto a screen in the back of the magnet (LCD projector: Epson America, Long Beach, CA). An oblique axial slice covering the primary visual cortex was chosen. Several protocols were performed, as follows:

1. A series of low- and high-resolution VASO and BOLD experiments were conducted to test the spatial characteristics of VASO. Block paradigms were used with 29.6-s ON periods interleaved with 29.6-s OFF periods. At the beginning of each scan, an extra OFF period (~1.5 min) was used to obtain more baseline points. Each functional scan contained five stimuli blocks. TR was 5920 ms, and 64 images were acquired. For low-resolution (voxel size = 4 × 4 × 10 mm^3) fMRI (five subjects (three females and two males), age range 20–32), a quadrature head coil was used for reception. Spatial Gaussian filters with full width at half maximum (FWHM) = 5 mm were applied. For high-resolution experiments (two subjects (one male and one female)) a surface coil was applied for reception and voxel sizes of 4 × 4 × 5 mm^3 and 2 × 2 × 5 mm^3 were used. T_1 maps corresponding to the two spatial resolutions were acquired using an inversion recovery pulse sequence. To preserve the high-resolution character of the data, no spatial filtering was applied.
2. A series of VASO, BOLD, and ASL experiments to compare the CNR and the temporal characteristics of the hemodynamic responses of the three methods (eight subjects (four males and four females, age range 20–39). The stimulation duration was 30 s, followed by a resting period of 50 s to allow complete settling of the hemodynamic response before the next trial. Each experiment consisted of three trials. Extra resting time (~30 s) was used at the beginning of each experiment. The parameters for the VASO, BOLD, and ASL experiments were identical: head coil reception, slice thickness = 5 mm, FOV = 240 × 240 mm^2, matrix = 64 × 64, TR = 2 s, and number of images acquired = 146. Spatial Gaussian filters (FWHM = 5 mm) were applied to improve the SNR.

Breath-Holding and Hyperventilation

Two male subjects (ages 32 and 46) were instructed to perform breath-holding (hypercapnia) or voluntary hyperventilation (hypocapnia) in two separate scans. The breath-holding/hyperventilation paradigm consisted of 20/40 s of task interleaved with 40/40 s of free breathing, and 6/4 repetitions. The scan parameters were: head coil reception, slice thickness = 5 mm, FOV = 240 × 240 mm^2, matrix = 64 × 64, TR = 2 s, and number of images = 201 (breath-holding) and 181 (hyperventilation). Spatial Gaussian filters (FWHM = 5 mm) were applied.

Data Processing

Complex images were reconstructed on the scanner and transferred to a Sun Enterprise server (SUN Microsystem, Mountain View, CA), where they were converted to mag-

nitude images. The images were realigned using the Automated Image Registration (AIR) algorithm (23). Images from the first ~25 s were discarded to allow the subject to get used to the scanner noise and reach a hemodynamic steady state. For each voxel time-course, a multilinear correction was performed to remove any baseline drift. For activation detection, the time-courses were correlated with a box-car function representing the stimulus paradigm. A statistical significance of $P < 0.005$ was used for all experiments, corresponding to the following thresholds: Visual stimulation protocol 1 used a cross-correlation coefficient (c.c.) for activation of ±0.22 ("+" for BOLD, "–" for VASO), cluster size 4, and SNR threshold 20. Protocol 2 had c.c. of ±0.18, cluster size 3, and SNR threshold 10 (protocol 2 has three times the number of points per unit measurement time than protocol 1, corresponding to a comparable SNR cutoff of 10 ($10 \cdot \sqrt{3} \approx 20$)); Breath-holding and hyperventilation paradigms used a c.c. of ±0.12, cluster size 3, and SNR threshold 10 (24). Signal time-courses were generated by averaging over all activated voxels and normalizing to the baseline signal. Note that because the stimulus onset was synchronized with the RF excitation pulse (not start of the sequence), the exact timing comparison of the ASL curves with the BOLD and VASO curves is not trivial. For BOLD and VASO, signal is based on what is present at the time of excitation, allowing a straightforward comparison to be made. For ASL (labeling, followed by 1.2 s of delay, followed by excitation and 0.8 s of recovery time), the flow image reflects the average blood flow during the two labeling periods. Thus, the point of comparison is at 1.6 s from the start of the first labeling, or 0.4 s after the start of the first excitation.

RESULTS

BOLD-fMRI and VASO-fMRI activation maps obtained during visual stimulation are shown in Fig. 2a and b. For both methods, clear activation can be seen in the part of the primary visual cortex corresponding to the central visual field. The BOLD data show a larger nmber of activated voxels than VASO-fMRI ($p < 0.005$), namely an average ($N = 5$) of 118 ± 16 vs. 57 ± 22, respectively. This difference is partly attributed to the lower SNR in the VASO case. Also, large venous vessels are known to cause extra activation areas in BOLD fMRI, which should not occur for the microvascular-based VASO-fMRI. The time-courses of the activated voxels are shown in Fig. 2c (BOLD) and d (VASO). At this low resolution of 4 × 4 × 10 mm^3, the BOLD signal increases by 1.5% during stimulation, while the VASO fMRI signal decreases by 0.7%.

In order to further validate the VASO method, experiments were performed using other physiological manipulations—breath-holding and hyperventilation, which are known to cause vasodilatation and vasoconstriction, respectively. As expected based on the VASO principles, breath-hold (hypercapnia) showed a negative signal change (Fig. 3a), while the response was positive during hyperventilation (hypocapnia) (Fig. 3b).

Figure 4a–c shows activation maps and hemodynamic responses acquired during visual activation using BOLD, VASO, and ASL, respectively. Similar activation regions can be seen in all techniques. VASO (68 ± 7 voxels) has lower sensitivity than BOLD (126 ± 11), but is comparable to ASL (61 ± 10). Since each technique reflects different physiological parameters (i.e., CBV for VASO, blood oxygenation for BOLD, and CBF for ASL), a comparison of their temporal characteristics provides insight into the dynamics of brain physiology during neuronal activation. Figure 4d shows the averaged hemodynamic responses ($N = 8$) of VASO (red), BOLD (blue), and ASL (black) fMRI. Note that the VASO signal time-course was inverted in display for easier comparison with the other two curves. VASO and ASL signals start to increase before the BOLD signal (Fig. 4d, brown arrow, $P < 0.005$), in agreement with previous reports of a BOLD onset latency of 2–3 s (25), and also indicating a significant arteriolar contribution to the total blood volume change. When the stimulus is stopped, the BOLD time-course rapidly drops to baseline, followed by a post-stimulus undershoot. The ASL curve drops simultaneously with BOLD, but does not show an undershoot. The VASO curve returns to baseline at a substantially slower pace (Fig. 4d, green arrow), in agreement with results from contrast-agent CBV studies on animals (26,27). These temporal characteristics (fast rise and slow decay) are consistent with the expected arteriolar and venular contributions in the VASO method.

To compare the spatial localization of VASO and BOLD, we performed fMRI and T_1 scans at a higher spatial resolution: voxel size = 2 × 2 × 5 mm^3 ($N = 2$). Activation maps, overlaid on a VASO image, are shown in Fig. 5a and b for BOLD and VASO, respectively. The averaged signal change for BOLD (262 voxels) was 2.70 ± 2.64(SD)%, whereas it was –2.15 ± 1.16(SD)% for the VASO experiments (146 voxels). Interestingly, the VASO effects (Fig. 5b) appear to be well localized to gray matter, while the BOLD effects (Fig. 5a) are still wide-spread, with the largest changes being close to the sagittal sinus. However, this difference in spatial distributions may simply be due to lower sensitivity in the VASO method. To separate the question of spatial specificy from effects of SNR, we constructed BOLD activation maps for the same number of activated voxels as in VASO (i.e., by increasing the threshold for BOLD to find the most activated 146 voxels), the results of which are shown in Fig. 5c. It can be seen that many BOLD voxels still overlap with the sulci. Since a VASO image (background images in Fig. 5a–c) displays clear contrast between gray matter, white matter, and blood, it can be used to identify voxel locations and tissue type. In the VASO image, the intensity of gray matter (in arbitrary units) was measured to be 3041 ± 699 (SD), while blood intensity was negligible (<200). When we analyzed the number-matched VASO- and BOLD-activated voxels, we found that only 1.4% of the VASO voxels had intensities that are 2 SD below gray matter (i.e., intensity < 1463), whereas this fraction was 13.7% for BOLD. An alternative way to distinguish gray matter voxels from blood vessels is to study the absolute T_1 image (Fig. 5d), in which each tissue type has a characteristic T_1value: 700 ms for white matter, 1000 ms for gray matter, 1350 ms for blood, and 4300 ms for CSF. Thus, by measuring the T_1 of the activated voxels, we can estimate the type of brain tissue it contains. The averaged T_1 values for BOLD- and VASO-activated voxels (Fig. 5b and c, with equal number of voxels) were 1103 ± 23 (SEM) ms and 1031 ± 20 (SEM) ms, respectively. The fact that the T_1 of the VASO-activated voxels was close to the nominal value for gray matter

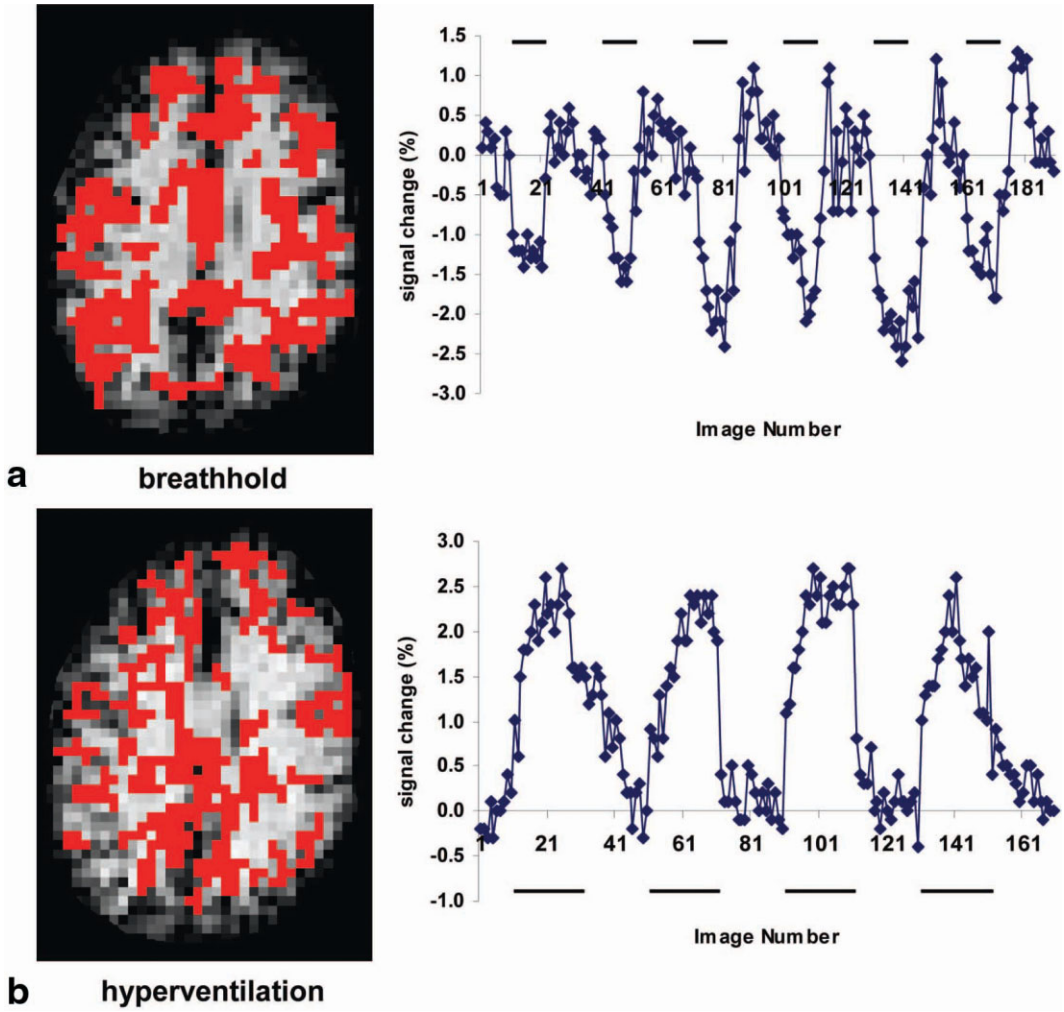

FIG. 3. VASO activation maps ($P < 0.005$) and hemodynamic response curves for breath-hold (hypercapnia) and hyperventilation (hypocapnia) experiments. Clear activation of gray matter relative to white matter can be seen, as expected based on the difference in CBV between these two tissues. In analogy to visual stimulation, VASO effects are negative during hypercapnia. During hypocapnia, the sign of the effect is reversed, consistent with a vasoconstriction. Dark lines indicate the period of activation.

(1000 ms) indicates a majority of gray matter as source of VASO fMRI signal, whereas BOLD voxels have larger T_1 values ($P < 0.03$), presumably due to partial voluming with large blood vessels.

Table 1 compares the CNR for all of the visual activation experiments. It can be seen that the VASO-CNR is lowest at low resolution (five times lower than BOLD), but improves at higher resolution (three times lower than BOLD, and comparable to ASL). This latter phenomenon is probably a result of reduced partial voluming with nonactivated brain tissue, and is consistent with the hypothesis of a higher spatial specificity for the VASO method.

DISCUSSION

The data in Figs. 2–5 and Table 1 show that the VASO method is a viable fMRI approach. During visual stimulation and breath-hold, the VASO signal is characterized by a signal decrease upon activation, excluding the possibility that the detected effect is an artifact due to residual BOLD-fMRI or vascular inflow effects, which would result in a signal increase. During hyperventilation the response is reversed, in agreement with the expectation of vasoconstriction. The VASO hemodynamic response (Fig. 4d) has a rapid rise, comparable to that of ASL methods, indicating an arteriolar contribution. The response decay, on the other hand, is delayed, which is comparable to results from animal CBV experiments with long-halflife blood tracers (26,27). These data are consistent with the hypothesis of a delayed postactivation venular compliance as described by Buxton et al. (25) and Mandeville et al. (28), which has been argued to be the source of the post-stimulus undershoot in the BOLD effect (e.g., Fig. 4d, blue curve). Thus, VASO has both arteriolar and venular components, in agreement with its presumed origin in the microvasculature. The CNR for VASO at a resolution of $3.75 \times 3.75 \times 5$ mm^3 and a TR value of 2 s is about three times smaller than that for BOLD, but is slightly higher than that for PASL approaches, as also reflected in the number of activated voxels.

VASO-fMRI complements BOLD-fMRI in the sense that it provides contrast depending on a single physiological parameter (CBV), while BOLD-fMRI signal reports on multiple parameters, including CBV and CBF (4,6,9,16). Based

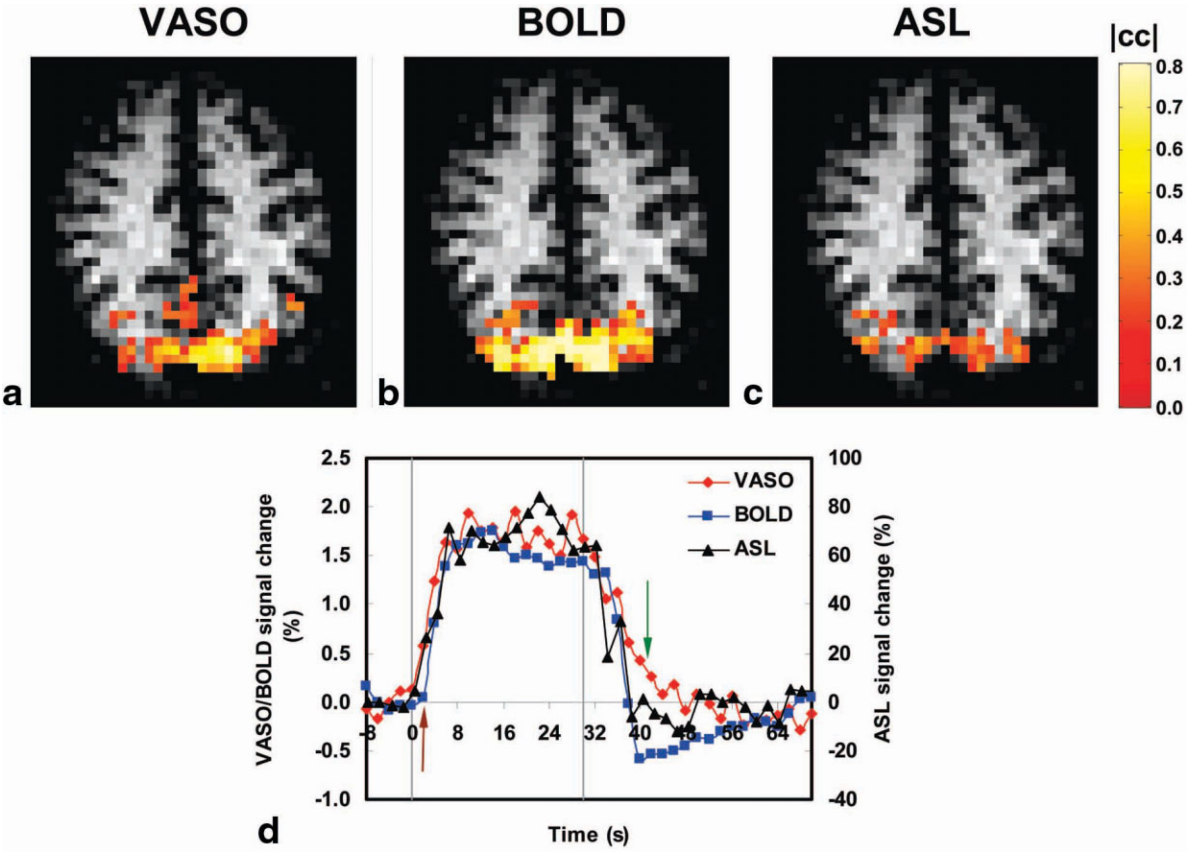

FIG. 4. Activation maps ($P < 0.005$) using VASO (**a**), BOLD (**b**), and ASL (**c**) fMRI during visual stimulation, and averaged (N = 8) hemodynamic responses (**d**). Color bar indicates the magnitude of the cross-correlation coefficient. Maps are overlaid on VASO-EPI images (64 × 64). Vertical gray lines indicate the start (0 s) and end (30 s) of the stimulus presentation. The VASO and ASL signals start to increase before the BOLD signal, while the VASO signal returns to baseline at a slower rate than the ASL signal. BOLD returns to baseline as fast as ASL, but continues with a post-stimulus undershoot.

on the literature for local vascular regulation (11,29), VASO-fMRI is expected to be sensitive to vessels smaller than 150–200 μm. For instance, it is well established that microvessels smaller than 200 μ are equipped with vascular smooth muscle cells and thus are able to constrict and dilate (30,31). This has been substantiated by scanning electron microscopy studies (29) showing that the only blood vessels capable of expanding or contracting are the smaller arterioles (diameter < ~80 μm), the capillaries, and only some of the smallest venules (diameter < ~100 μm). Recently, using in vivo videomicroscopy, Lee et al. (32) measured changes in diameter of vessels with initial calibers of 20, 30, and 40 μm under hypercapnia. Their results showed that the diameter of the arterioles increased more (58%, 44%, 29%, respectively) than that of the venous vessels (11%, 7%, 4%, respectively). If we extrapolate their data to higher diameters, assuming exponential scaling, arterial vessels larger than 135 μm would have a diameter increase of <1%, which corresponds to a volume increase of 2%. Assuming a typical microvascular CBV of about 5% in gray matter (15), the measured 2.15% decrease in tissue volume would be translated to an increase in CBV of 46% (at a voxel size of 2 × 2 × 5 mm^3). This corresponds to a diameter increase of about 20%, which is not unreasonable in view of the measured size changes quoted above. Our estimation of a CBV increase of 46% is somewhat higher than previous results using paramagnetic contrast agent (33) (~30%), probably because of the higher spatial resolution used in the current study (2 × 2 × 5). A similar observation has been made in high-resolution CBF measurements (34). Thus, within the limits of current typical fMRI spatial resolution (several mm), and based on its vascular size base, the VASO-fMRI changes are expected to be well localized to the region of neuronal activity.

Unfortunately, it is not easy to provide a "gold standard" showing that VASO localization is specific to the parenchyma. However, the results of this study provide several supporting arguments. First, when the numbers of activated VASO and BOLD voxels are matched in an fMRI experiment (i.e., a higher BOLD threshold is chosen to compensate for BOLD's higher sensitivity (Fig. 5c)), the VASO approach shows excellent localization in gray matter (>98.6%), while BOLD still shows many voxels (13.7%) in the sulci (dark regions in the background VASO image), where the large vessels reside. Second, when the T_1 values are analyzed for these activated voxels, a longer T_1 is found for the BOLD voxels compared to the VASO voxels, in agreement with the longer T_1 values for venous blood known to contribute to the BOLD voxels at 1.5T. Third, when going from low to high resolution, the signal change increases drastically in VASO (from 0.7% to 2.2%),

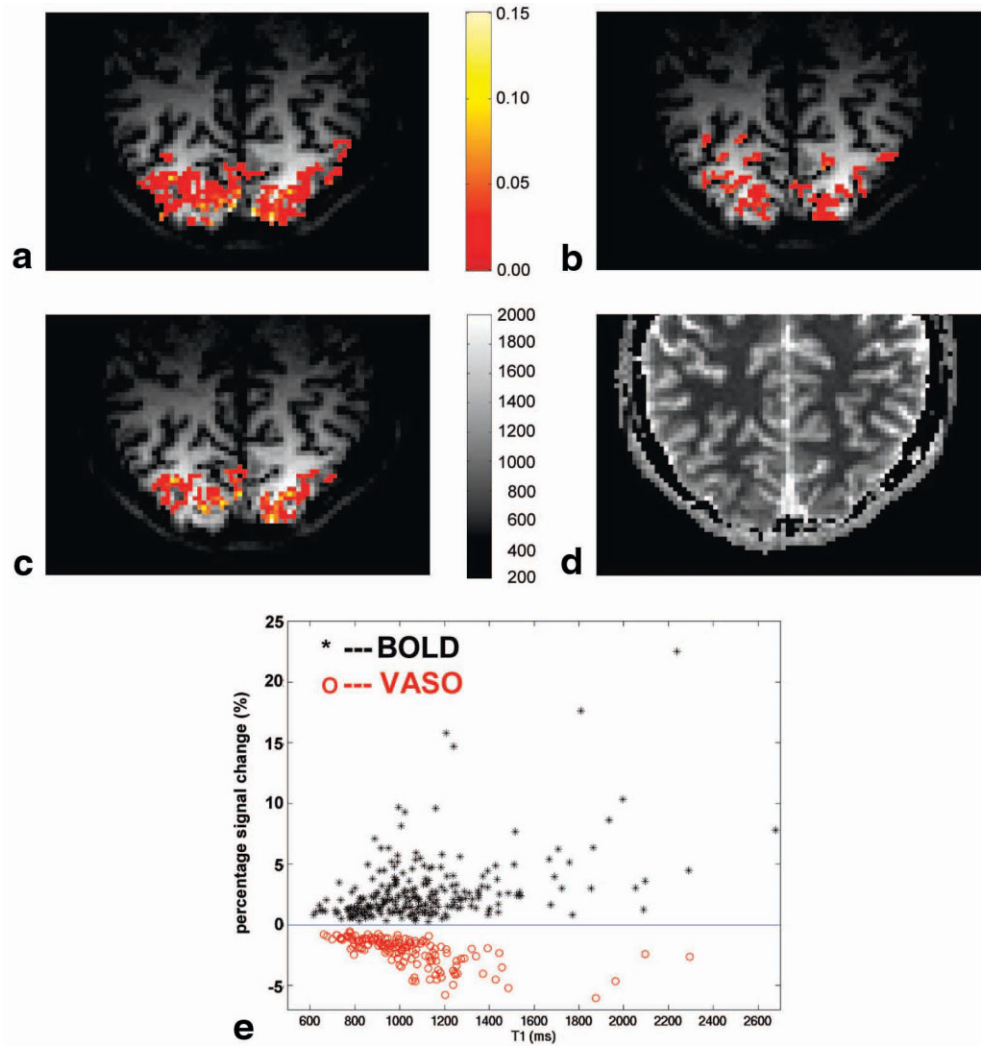

FIG. 5. Comparison of spatial localizations between BOLD (**a** and **c**) and VASO (**b**) activation maps. Absolute T_1 maps showing gray matter (gray), white matter (dark), and CSF regions (sulci, bright) are given for comparison (**d**). Scatter plots of fractional signal changes vs. T_1 are also shown in **e**. Resolution: $2 \times 2 \times 5$ mm^3. Using the same c.c. threshold, the number of activated voxels in BOLD (**a**) is larger than in VASO (**b**), which does not necessarily prove a higher spatial specificity for VASO. Therefore, in **c**, the number of BOLD voxels was matched to the VASO number by choosing a higher threshold for activation. Under these matched conditions, the VASO approach shows excellent localization in gray matter (>98.6%), while BOLD still shows many voxels (13.7%) in the sulci (dark regions in the background VASO image).

but not in BOLD. We attribute this to severe partial voluming with nonactivated regions at lower resolution in VASO. Such an increase does not occur in BOLD, because many regions remain activated at low resolution due to partial voluming with draining veins, where the oxygenation effects upon activation are much larger than in the tissue. A similar pattern (i.e., a dramatic increase in signal change when going to high resolution) was also seen in a recent study on CBF fMRI (34), which is also thought to be a parenchyma-specific method. At high resolution, parenchyma and veins can be studied separately, since they show very large BOLD effects in the large vessels and smaller effects in parenchyma. The size distribution for VASO is more homogeneous (Fig. 5e), with all effects being <6%, while BOLD effects as large as 22.5% are found.

Table 1
Contrast-to-Noise Ratio (CNR)* Comparison Between Oxygenation-Based (BOLD), CBV-Based (VASO), and CBF-Based (TILT, Pulsed Arterial Spin Labeling) fMRI for Visual Stimulation Experiments at Different Temporal and Spatial Resolutions at 1.5 T

TR (s)	Resolution (mm^3)	BOLD	VASO	TILT
5.92	$2 \times 2 \times 5^a$	30.4	9.7	–
	$4 \times 4 \times 5^a$	51.9	11.8	–
	$4 \times 4 \times 10^b$	44.3	8.7	–
2.00	$3.75 \times 3.75 \times 5^b$	21.4	7.0	6.5

*CNR = SNR × signal change (%) × $\sqrt{\text{number of images}}$.
[a]Surface coil used for reception.
[b]Quadrature head coil used for reception.

Physiological Considerations

These first VASO-fMRI data provide new insights into fundamental questions concerning vascular regulation during functional stimulation. A first point relates to the longstanding question of how parenchymal water redistributes between tissue and vasculature during local CBV increase, an issue that cannot be addressed by present blood volume imaging approaches (26,33,35). Assuming equal perfusion of all microvessels, the two possible extreme situations are: 1) tissue volume decreases, but tissue water volume remains the same due to compliance of the tissue; and 2) tissue water volume decreases proportionally to the tissue volume decrease, by relocating tissue water to the blood compartment. In the first situation, zero VASO signal change is expected upon activation, while in the second situation, a negative VASO effect is predicted.

Table 2
Parameters Used for the Numerical Simulations in the Appendix

Physiological state	P (ml/100g/min)	E	C_{blood} (g/ml)	C_{tissue} (g/ml)	D_{par} (g/ml)	$T_{1,blood}$ (ms)	$T_{1,tissue}$ (ms)	ξ (%)	L
Resting state	60[a]	0.5[c]	0.87[e]	0.89[e]	1.06[f]	1400[e]	1000[e]	4.59[e]	1[h]
Activated state	102[b]	0.85[d]	0.87[e]	0.89[e]	1.06[f]	1400[e]	1000[e]	6.20[g]	1[h]

[a]From Ref. 11.
[b]Based on 70% of CBF change.
[c]From Ref. 39.
[d]Proportional to CBF increase.
[e]From Ref. 16.
[f]From Ref. 40.
[g]Based on 35% of CBV change.
[h]Assume homogeneous capillary distribution.

Thus, our new approach can be used to directly investigate the basic principles of water distribution during functional activation. The negative signal change measured with VASO-fMRI is consistent with a relocation of water from the tissue to the vasculature during visual stimulation.

A second point relates to a number of reports (36,37) that some, but not all, capillaries are perfused with whole blood, and that about 10% of capillaries are perfused with plasma alone or not at all. According to these reports, activation or hypercapnia causes erythrocytes to be recruited to these parts of the microcirculation, leading to a more homogeneous flow pattern. This capillary recruitment theory would lead to only very small changes in CBV, and is therefore not consistent with our findings in the VASO experiment.

Technical Considerations

While VASO-fMRI has certain potential advantages compared to BOLD-fMRI (e.g., a simple relation between the signal and a physiological parameter (CBV), fast initial response, and expected better spatial localization), it also has several disadvantages. The most obvious one is a limitation in SNR, which is 2–2.5 times lower than in BOLD. Although some SNR is gained back by the use of short TEs, we found a CNR loss by a factor of about 3 at the common fMRI resolution ($3.75 \times 3.75 \times 5$ mm^3). However, significant activations were detected in all VASO experiments. Potential approaches to increase the SNR include the use of a phased-array head coil, spiral acquisition for shorter TE, and higher field strength.

The data interpretation of the VASO experiments is based on the assumption that the extravascular BOLD effect does not contribute significantly at short TE, and that there is negligible contamination of CSF in the voxel. In order to verify the minimal effects of BOLD at the short TE used, we performed some VASO-fMRI experiments as a function of TE (TE = 10, 30, 50, 70, 90, and 100 ms) and calculated the residual extravascular BOLD effect on the relaxation time of the tissue. For the activation threshold range used (c.c = 0.20–0.25), T_2^* of tissue increased by 0.26–0.30 ms going from a resting to an activated state. In terms of magnitude of signal change ($[1/T_{2par}^{*,act} - 1/T_{2par}^{*,rest}]$TE), this corresponds 0.066–0.075% at TE = 11 ms, which is much smaller than the –1.7% of the VASO signal change. A second potential problem may be that the long echo trains could have BOLD contributions at the higher TE locations. The echo train lengths for each resolution were: 23 ms for $4 \times 4 \times 10$, 24 ms for $3.75 \times 3.75 \times 5$, 15 ms for $4 \times 4 \times 5$, and 47 ms for $2 \times 2 \times 5$. Using the above T_2^* change for an effective TE of 50 ms, the maximal residual BOLD effect is still only 0.3%, which is still much less than the VASO signal. Also, as the higher phase encodings contribute less signal, the contribution is expected to be less than this maximum. However, this situation may have to be reevaluated at higher fields, where the BOLD effect is stronger.

As far as the second assumption is concerned, partial voluming with CSF will complicate the quantification of CBV changes, in that the presence of CSF in the voxel will result in an overestimation of the relative CBV change. At the time of image acquisition, the tissue signal is positive, blood signal is zero, and CSF signal is negative. If the CBV increase were at the cost of CSF space, this would lead to an increase in VASO signal. In our VASO experiments, negative signal changes were consistently observed. Thus it is not likely that CSF space changes caused the VASO signal. In order to understand the effects under different possible conditions, we performed simulations using three starting conditions: 1) no CSF in voxel; 2) 5% CSF in voxel, and CSF space does not change; and 3) 5% CSF in the voxel, and CSF space decreases instead of tissue space. These conditions led to signal changes of –1.59%, –1.82%, and +2.83%, respectively. The second condition could increase the VASO effect, while the third could reduce it. In our high-resolution data, we found that the VASO-activated voxels had smaller T_1 values than the BOLD voxels. Considering that CSF has a relatively long T_1 (4300 ms), we do not expect a major contribution from CSF in the VASO signal.

It may be a matter of concern that, as a consequence of proton exchange between the tissue and capillary compartments, the nulling of blood spins may not be perfect in the capillaries and initial part of venules, resulting in a residual signal in the blood compartment. To verify whether such exchange would influence the VASO experiment, we constructed a parenchymal model containing four pools: 1) spins that were originally in blood but later entered tissue, 2) spins that were originally in tissue and later entered blood, and spins that remained in 3) tissue and 4) blood during the total period TI. The details of this model are presented in the Appendix, along with numerical simulations performed using literature values (Table 2) for the physiological constants and relaxation times. When increases in extraction fraction in proportion to the

measured increases in CBF during activation are assumed, the VASO signal changes with and without the effect of increased exchange are –1.77% and –1.79%, respectively, suggesting that the capillary exchange rate has negligible effects on the overall VASO signal.

Finally, functional imaging generally requires the acquisition of multiple slices, and therefore VASO methods must be developed in which blood signal can remain negligible over a prolonged period of time.

Comparison With Current CBV-Based fMRI Methods

Previous CBV-based fMRI studies (26,28,33,38) used exogenous contrast agents. The VASO technique is completely noninvasive and can be performed repetitively on awake humans. Most of the recent contrast agent-based CBV-fMRI studies were conducted on anesthetized animals and used long halflife paramagnetic particles for blood labeling (26,28,38). Similar to deoxyhemoglobin in BOLD, paramagnetic vascular agents have extravascular T_2^* effects, and localization of activation is not straightforward. However, VASO uses the T_1 characteristics of blood, and its labeling effect at short TE is limited to intravascular spins.

CONCLUSIONS

The spatial specificity of BOLD fMRI is confounded by signal changes in and around large venous vessels. In the search for an MRI brain mapping technique with better localization, VASO-fMRI is a prospective candidate. The new technology can be easily implemented on standard clinical systems, and its signal reflects changes of a single physiological parameter (CBV). Furthermore, VASO-fMRI data acquisition can be done at short TE and with all possible image schemes (e.g., spin echoes can be used instead of gradient echoes, thus avoiding magnetic susceptibility-based image distortions, such as those occurring close to the sinuses and in the temporal lobe). This will be especially important at higher fields and when this new technology is applied to other organs. One disadvantage of VASO-fMRI is the limited SNR. However, improved sensitivity is expected from the use of higher magnetic field strengths and multi-array coils. The simplicity of the contrast mechanism and the expectation of better spatial localization may make VASO a useful alternative for fMRI studies. In addition to providing a new approach for fMRI, the VASO-MRI technique also has potential as a noninvasive alternative for blood volume MRI studies, as it allows such studies to be repeated within the same MRI session (such as when studying time-dependent CBV changes). For example, CBV studies would be useful for imaging of acute stroke, cardiac ischemia, and tumor angiogenesis.

ACKNOWLEDGMENTS

Johanna Silvennoinen and Chekesha Clingman are acknowledged for their help with the blood perfusion studies. We are grateful to Dr. Jean-Francois Payen for helpful discussions. Dr. Golay was supported in part by a grant from Philips Medical Systems.

APPENDIX

VASO Model Considering Proton Exchange

To consider proton exchange in VASO experiments, a two-pool model is insufficient, and the parenchymal protons must be divided into four different pools. These consist of 1) spins originally in blood but exchanged to tissue, 2) spins originally in tissue but exchanged to blood, 3) spins remaining in tissue during the total length of TI, and 4) spins remaining in blood. The total parenchymal signal is the sum of the signal contributions from these pools. Each individual pool is evaluated below.

1. *Spins Originally in Blood but Exchanged to Tissue*

The general solution to the Bloch equation without B_1 contribution is given by:

$$M(t) = 1 + K \cdot \exp(-t/T_1) \quad [A1]$$

where $M(t)$ is the magnetization as a function of time t, T_1 is the longitudinal relaxation time, and K is a constant determined by initial conditions. All spins are assumed to be in steady state before the inversion pulse. Assuming perfect inversion efficiency (we used a hyperbolic-secant adiabatic pulse), the initial condition is given by $M(0) = -(1 - \exp(-(\mathrm{TR} - \mathrm{TI})/T_1))$. Thus, $K = \exp(-(\mathrm{TR} - \mathrm{TI})/T_1) - 2$.

The longitudinal recovery after inversion depends on the environment in which the spin resides, namely, the tissue compartment or blood compartment. For a spin exchanging from blood to tissue at time t, the magnetization at the time of exchange is given by $M(t) = 1 + (\exp(-(\mathrm{TR} - \mathrm{TI})/T_{1,blood}) - 2) \cdot exp(-t/T_{1,blood})$. The magnetization at excitation can then be calculated to be:

$$M(\mathrm{TI}) = 1 + (\exp(-(\mathrm{TR} - \mathrm{TI})/T_{1,blood}) - 2) \cdot \exp(-t/T_{1,blood}) \cdot \exp(-(\mathrm{TI} - t)/T_{1,tissue}) \quad [A2]$$

The signal from this spin pool can be obtained by integrating over all exchanged spins from time 0 to the end of TI:

$$S_1 = \int_0^{\mathrm{TI}} [1 + (\exp(-(\mathrm{TR} - \mathrm{TI})/T_{1,blood}) - 2) \cdot \exp(-t/T_{1,blood}) \cdot \exp(-(\mathrm{TI} - t)/T_{1,tissue})] \cdot P \cdot E \cdot C_{blood} \cdot D_{par} \cdot dt \quad [A3]$$

where P is the perfusion of the parenchyma in ml of blood/g parenchyma/ms, E is the fraction of spins exchanged into tissue, and D_{par} is the density of parenchyma in g/ml.

2. *Spins Originally in Tissue but Exchanged to Blood*

This calculation is similar to the spins exchanging the opposite way. However, once they enter the blood compartment, the spins may flow out of the imaging slice, and a probability-based outflow factor must be considered in the model. Because spins entering the blood compartment at the beginning of TI have a greater chance to leave the imaging slice, we modeled the time-dependent probability for a blood spin to leave the slice as $l(t) = L - (L/\mathrm{TI}) \cdot t$ (Fig. 6), where L is the maximum probability for a spin to leave the imaging slice. The signal is then given by:

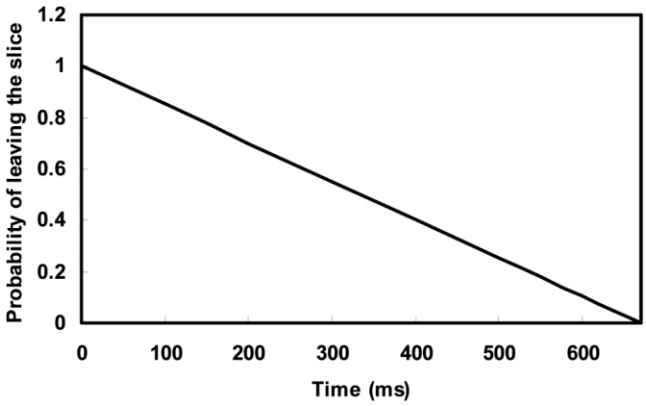

FIG. 6. Probability of a spin to leave the imaging slice as a function of time of exchange. A linear decrease in probability was assumed. The spins exchanging into the blood compartment at the end of TI (i.e., t = TI) have zero probability of leaving the imaging slice. Spins exchanging immediately after inversion (i.e., t = 0) have maximum probability L. An L of 1 was assumed.

$$S_2 = \int_0^{\mathrm{TI}} [1 + (\exp(-(\mathrm{TR} - \mathrm{TI})/T_{1,tissue}) - 2) \cdot \exp(-t/T_{1,tissue}) \cdot \exp(-(\mathrm{TI} - t)/T_{1,blood})] \cdot P \cdot E \cdot C_{blood} \cdot D_{par} \cdot \left(1 - L + \frac{L}{\mathrm{TI}}\, t\right) \cdot dt \quad [A4]$$

3. *Spins Remaining in the Tissue During TI*

The magnetization of the static spins at TI is similar to Eq. [A2], except that $T_{1,blood}$ should be replaced by $T_{1,tissue}$, which leads to:

$$M(\mathrm{TI}) = 1 + (\exp(-(\mathrm{TR} - \mathrm{TI})/T_{1,tissue}) - 2) \cdot \exp(-\mathrm{TI}/T_{1,tissue}). \quad [A5]$$

The signal is then given by:

$$M(\mathrm{TI}) = [1 + (\exp(-(\mathrm{TR} - \mathrm{TI})/T_{1,tissue}) - 2) \cdot \exp(-\mathrm{TI}/T_{1,tissue})] \cdot ((C_{par} - \xi \cdot C_{blood}) - P \cdot E \cdot C_{blood} \cdot D_{par} \cdot \mathrm{TI}) \quad [A6]$$

where ξ is the total vascular space occupancy of the voxel (see Theory).

4. *Spins Remaining in Blood During TI*

When spins flowing into the slice to replace the exchanged spins that leave the imaging slice (see pool 2) are taken into account, the signal from the blood spins that remain in the blood during TI is:

$$S_4 = [1 + (\exp(-(\mathrm{TR} - \mathrm{TI})/T_{1,blood}) - 2) \cdot \exp(-\mathrm{TI}/T_{1,blood})] \cdot \left(\xi \cdot C_{blood} - P \cdot E \cdot C_{blood} \cdot D_{par} \cdot \mathrm{TI} \cdot \frac{2 - L}{2}\right) \quad [A7]$$

The total signal in the voxel is given by:

$$S_{total} = S_1 + S_2 + S_3 + S_4 \quad [A8]$$

Using parameter values from the literature (Table 2), the expected signal changes during activation with ($E > 0$) and without ($E = 0$) proton exchange can be calculated. Using changes in E in proportion to the measured changes in CBF, the signal changes with and without the effect of increased exchange are –1.77% and –1.79%, respectively, which suggests that the capillary exchange rate has negligible effects on the overall VASO signal.

REFERENCES

1. Ogawa S, Tank DW, Menon R, Ellermann JM, Kim SG, Merkle H, Ugurbil K. Intrinsic signal changes accompanying sensory stimulation: functional brain mapping with magnetic resonance imaging. Proc Natl Acad Sci USA 1992;89:5951–5955.
2. Kwong KK, Belliveau JW, Chesler DA, Goldberg IE, Weisskoff RM, Poncelet BP, Kennedy DN, Hoppel BE, Cohen MS, Turner R, Cheng HM, Brady TJ, Rosen BR. Dynamic magnetic resonance imaging of human brain activity during primary sensory stimulation. Proc Natl Acad Sci USA 1992;89:5675–5679.
3. Bandettini PA, Wong EC, Hinks RS, Tikofsky RS, Hyde JS. Time course EPI of human brain function during task activation. Magn Reson Med 1992;25:390–397.
4. Ogawa S, Menon RS, Tank DW, Kim SG, Merkle H, Ellermann JM, Ugurbil K. Functional brain mapping by blood oxygenation level-dependent contrast magnetic resonance imaging. A comparison of signal characteristics with a biophysical model. Biophys J 1993;64:803–812.
5. Turner R, Le Bihan D, Moonen CT, Despres D, Frank J. Echo-planar time course MRI of cat brain oxygenation changes. Magn Reson Med 1991;22:159–166.
6. van Zijl PC, Eleff SM, Ulatowski JA, Oja JM, Ulug AM, Traystman RJ, Kauppinen RA. Quantitative assessment of blood flow, blood volume and blood oxygenation effects in functional magnetic resonance imaging. Nat Med 1998;4:159–167.
7. Lai S, Hopkins AL, Haacke EM, Li D, Wasserman BA, Buckley P, Friedman L, Meltzer H, Hedera P, Friedland R. Identification of vascular structures as a major source of signal contrast in high resolution 2D and 3D functional activation imaging of the motor cortex at 1.5T: preliminary results. Magn Reson Med 1993;30:387–392.
8. Frahm J, Merboldt K-D, Hänicke W. Functional MRI of human brain activation at high spatial resolution. Magn Reson Med 1993;29:139–144.
9. Gati JS, Menon RS, Ugurbil K, Rutt BK. Experimental determination of the BOLD field strength dependence in vessels and tissue. Magn Reson Med 1997;38:296–302.
10. Oja JME, Gillen JS, Kauppinen RA, Kraut M, van Zijl PCM. Venous blood effects in spin echo fMRI of human brain. Magn Reson Med 1999;42:617–627.
11. Kuschinsky W. Regulation of cerebral blood flow: an overview. In: Mraovitch S, Sercombe R, editors. Neurophysiological basis of cerebral blood flow control: an introduction. London: Johns Libbey & Company Ltd.; 1996. p 245–262.
12. Gally JA, Montague PR, Reeke Jr GN, Edelman GM. The NO hypothesis: possible effects of a short-lived, rapidly diffusible signal in the development and function of the nervous system. Proc Natl Acad Sci USA 1990;87:3547–3551.
13. Wagerle LC, Mishra OP. Mechanism of CO2 response in cerebral arteries of the newborn pig: role of phospholipase, cyclooxygenase, and lipoxygenase pathways. Circ Res 1988;62:1019–1026.
14. Brooks RA, Di Chiro G. Magnetic resonance imaging of stationary blood: a review. Med Phys 1987;14:903–913.
15. Tomita M. Significance of cerebral blood volume. In: Tomita M, Sawada T, Naritomi H, editors. Cerebral hyperemia and ischemia: from the standpoint of cerebral blood volume. New York: Elsevier Science Publisher; 1988. p 3–30.
16. Lu H, Golay X, van Zijl PC. Inter-voxel heterogeneity of event-related fMRI responses as a function of T1-weighting. NeuroImage 2002;17:943–955.
17. Meyer ME, Yu O, Eclancher B, Grucker D, Chambron J. NMR relaxation rates and blood oxygenation level. Magn Reson Med 1995;34:234–241.

18. Golay X, Silvennoinen MJ, Zhou J, Clingman CS, Kauppinen RA, Pekar JJ, van Zijl PC. Measurement of tissue oxygen extraction ratios from venous blood T(2): increased precision and validation of principle. Magn Reson Med 2001;46:282–291.
19. Benga G, Borza T. Diffusional water permeability of mammalian red blood cells. Comp Biochem Physiol B Biochem Mol Biol 1995;112:653–659.
20. Perman WH, el-Ghazzawy O, Gado MH, Larson KB, Perlmutter JS. A half-Fourier gradient echo technique for dynamic MR imaging. Magn Reson Imaging 1993;11:357–366.
21. Golay X, Stuber M, Pruessmann KP, Meier D, Boesiger P. Transfer insensitive labeling technique (TILT): application to multislice functional perfusion imaging. J Magn Reson Imaging 1999;9:454–461.
22. Edelman RR, Siewert B, Darby DG, Thangaraj V, Nobre AC, Mesulam MM, Warach S. Qualitative mapping of cerebral blood flow and functional localization with echo-planar MR imaging and signal targeting with alternating radio frequency. Radiology 1994;192:513–520.
23. Woods RP, Grafton ST, Holmes CJ, Cherry SR, Mazziotta JC. Automated image registration: I. General methods and intrasubject, intramodality validation. J Comput Assist Tomogr 1998;22:139–152.
24. Bandettini PA, Jesmanowicz A, Wong EC, Hyde JS. Processing strategies for time-course data sets in functional MRI of the human brain. Magn Reson Med 1993;30:161–173.
25. Buxton RB, Wong EC, Frank LR. Dynamics of blood flow and oxygenation changes during brain activation: the balloon model. Magn Reson Med 1998;39:855–864.
26. Mandeville JB, Marota JJ, Kosofsky BE, Keltner JR, Weissleder R, Rosen BR, Weisskoff RM. Dynamic functional imaging of relative cerebral blood volume during rat forepaw stimulation. Magn Reson Med 1998; 39:615–624.
27. Leite FP, Tsao D, Vanduffel W, Fize D, Sasaki Y, Wald LL, Dale AM, Kwong KK, Orban GA, Rosen BR, Tootell RB, Mandeville JB. Repeated fMRI using iron oxide contrast agent in awake, behaving macaques at 3 Tesla. Neuroimage 2002;16:283–294.
28. Mandeville JB, Marota JJ, Ayata C, Zaharchuk G, Moskowitz MA, Rosen BR, Weisskoff RM. Evidence of a cerebrovascular postarteriole windkessel with delayed compliance. J Cereb Blood Flow Metab 1999;19: 679–689.
29. Harrison RV, Harel N, Panesar J, Mount RJ. Blood capillary distribution correlates with hemodynamic-based functional imaging in cerebral cortex. Cereb Cortex 2002;12:225–233.
30. Duelli R, Kuschinsky W. Changes in brain capillary diameter during hypocapnia and hypercapnia. J Cereb Blood Flow Metab 1993;13:1025–1028.
31. Atkinson JL, Anderson RE, Sundt Jr TM. The effect of carbon dioxide on the diameter of brain capillaries. Brain Res 1990;517:333–340.
32. Lee SP, Duong TQ, Yang G, Iadecola C, Kim SG. Relative changes of cerebral arterial and venous blood volumes during increased cerebral blood flow: implications for BOLD fMRI. Magn Reson Med 2001;45: 791–800.
33. Belliveau JW, Kennedy Jr DN, McKinstry RC, Buchbinder BR, Weisskoff RM, Cohen MS, Vevea JM, Brady TJ, Rosen BR. Functional mapping of the human visual cortex by magnetic resonance imaging. Science 1991;254:716–719.
34. Pfeuffer J, Adriany G, Shmuel A, Yacoub E, Van De Moortele PF, Hu X, Ugurbil K. Perfusion-based high-resolution functional imaging in the human brain at 7 Tesla. Magn Reson Med 2002;47:903–911.
35. Ostergaard L, Smith DF, Vestergaard-Poulsen P, Hansen SB, Gee AD, Gjedde A, Gyldensted C. Absolute cerebral blood flow and blood volume measured by magnetic resonance imaging bolus tracking: comparison with positron emission tomography values. J Cereb Blood Flow Metab 1998;18:425–432.
36. Hudlicka O, Zweifach BW, Tyler KR. Capillary recruitment and flow velocity in skeletal muscle after contractions. Microvasc Res 1982;23: 201–213.
37. Chen JL, Wei L, Acuff V, Bereczki D, Hans FJ, Otsuka T, Finnegan W, Patlak C, Fenstermacher J. Slightly altered permeability-surface area products imply some cerebral capillary recruitment during hypercapnia. Microvasc Res 1994;48:190–211.
38. van Bruggen N, Busch E, Palmer JT, Williams SP, de Crespigny AJ. High-resolution functional magnetic resonance imaging of the rat brain: mapping changes in cerebral blood volume using iron oxide contrast media. J Cereb Blood Flow Metab 1998;18:1178–1183.
39. Zhou J, Wilson DA, Ulatowski JA, Traystman RJ, van Zijl PC. Two-compartment exchange model for perfusion quantification using arterial spin tagging. J Cereb Blood Flow Metab 2001;21:440–455.
40. Herscovitch P, Raichle ME. What is the correct value for the brain–blood partition coefficient for water? J Cereb Blood Flow Metab 1985; 5:65–69.